State-selective electron capture in $He^+ + H_2$ collisions at intermediate impact energies

M. Alessi,[1] N. D. Cariatore,[2] P. Focke,[1] and S. Otranto[2]

[1]*Comisión Nacional de Energía Atómica, Centro Atómico Bariloche, Avenida E. Bustillo 9500, 8400 Bariloche, Argentina*

[2]*IFISUR and Departamento de Física, Universidad Nacional del Sur, 8000 Bahía Blanca, Argentina*

(Received 20 December 2011; published 5 April 2012)

State-selective single electron capture in collisions of He^+ with H_2 molecules is investigated using the cold-target recoil-ion momentum spectroscopy technique. The energy range considered is 6.25 keV/amu (projectile velocity $v_p = 0.5$ a.u.) to 50 keV/amu ($v_p = 1.41$ a.u.). In addition, we explore the transverse recoil momentum distributions that provide direct access to the angular scattering of the receding projectile. The present experimental data are contrasted to the theoretical results obtained by means of the classical trajectory Monte Carlo model with which we find good overall agreement in the energy range explored.

DOI: 10.1103/PhysRevA.85.042704 PACS number(s): 34.70.+e, 34.10.+x, 34.50.−s

I. INTRODUCTION

Despite the great advances achieved in past decades in experimental devices and techniques as well as in the development and improvement of the existing theoretical models, the study of ion collisions with molecular targets still represents an area that remains, to a great extent, unexplored. Particular interest in these collision systems arises from their potential role in diverse areas, such as radiobiology and astrophysics. For the former, we note that different cross sections are needed to feed statistical methods that track the energy deposition [1]. For the latter, we can cite the recent discovery of the cometary x-ray emission, which is originated by charge-exchange processes between the solar wind ions and the cometary gases in the comet coma [2,3]. The same mechanism was later on found to apply to planetary atmospheres as well.

Additionally, since the 1970s, the tokamak fusion plasma program has prompted the experimental and theoretical determination of charge-exchange cross sections. Photon emission after electron capture on hydrogen targets has been used in tokamaks as a diagnostic tool for the impurity ion concentrations, the temperature, and the rotation of the plasma [4]. An additional role is yet deserved for charge-exchange reactions in the ITER program actually under construction in Cadarache (France) [5]. It is expected that charge exchange by highly charged ions followed by photon emission would possibly remove the risk of heat localization in the divertors and the plasma facing walls.

The need for highly differential cross sections for charge-exchange and ionization processes in different fields prompted the development of innovative experimental techniques. The cold-target recoil-ion momentum spectroscopy (COLTRIMS) methodology, developed by the Frankfurt and Heidelberg groups in the mid-1990s [6] provided (via incorporation of supersonic jets, cold targets, and measurements in coincidence between the projectile and the reaction fragments), a new perspective for the exploration of collision processes on atoms and molecules by ions, electrons, and photons by means of kinematically complete experiments [7,8]. Many papers that were considered prohibitive up to then, such as the determination of state-selective charge-exchange cross sections in ion-atom collisions or the study of collision processes at the impact parameter level became technically feasible [9,10]. An additional advantage of the aforementioned setup is its ductility. Besides charge-exchange processes, ionization processes (single and multiple) at the fully differential level by charged particles or photons have been studied throughout the years ([11–13] and references therein).

More recently, a COLTRIMS method in which the cold target is provided by means of laser cooling and trapping has been developed. This method has been termed MOTRIMS (for magneto-optical trap recoil-ion momentum spectroscopy) to distinguish it from the classical COLTRIMS setup [14–16]. In a recent experimental breakthrough, the KVI group presented benchmark state-selective charge-exchange data for Xe^{18+} ions colliding with Na($3s$), measured using the MOTRIMS method [17,18]. These papers are expected to provide good estimates on the charge-exchange cross sections for the elusive $H^*(n = 2)$ target of particular importance for the fusion reactor program. As a result, and in view of the potential capabilities of the COLTRIMS technique, during the past decade, several laboratories worldwide started to work on their own devices.

The study of charge-exchange collisions, besides its interest in the applications before mentioned, is also of relevance for the intrinsic understanding of many-body rearrangement collisions. In this respect, experimental work provides valuable information that may be useful to benchmark theoretical models. In this context, it is of great interest to study the relative simple systems, consisting of light projectiles colliding on simple targets. Being the simplest neutral molecule, H_2 has received a lot of attention from the experimental point of view. Early experimental papers focused on the determination of absolute total cross sections and were based on the same spectroscopic methods used to study ionization and fragmentation processes [19–23]. Some laboratories were able to separate the contributions of single-electron capture arising from different electron-loss channels [24]. A number of measurements has been performed on molecular and atomic targets with the completely ionized projectile He^{2+} [25–33] to mention a few. Some used traditional techniques to obtain total cross sections, while others used photon-emission spectroscopy that allowed the study of the excited capture channels and translational energy spectroscopy for the detection of all capture channels.

In this paper, our aim is to use the COLTRIMS setup mounted at the atomic physics laboratory in Bariloche (Argentina) to explore single charge-exchange reactions in

$He^+ + H_2$ collisions at the impact parameter level and to test the results with classical trajectory Monte Carlo (CTMC) calculations. This simple system, consisting of a structured projectile and the simplest diatomic molecule, represents a challenging field for theoretical modeling. Earlier theoretical and experimental work on single charge-exchange collisions for this system has been reviewed in Ref. [34] for the intermediate-energy regime where the relative collision velocity is lower than the electron orbital velocity. The experimental work was performed in the frame of optical and collision spectroscopy methods. COLTRIMS experiments were more intensively concentrated on the study of collision processes involving highly charged and bare ionic projectiles. Related state-selective studies to the present system were performed with hydrogenlike and He-like projectiles [35,36].

For the present collision system, there are four possible channels leading to the capture of one electron by the projectile,

$$He^+ + H_2 \rightarrow He^0(n) + H_2{}^+(1s\sigma_g) \quad \text{[single capture (SC)]} \tag{1}$$

$$He^+ + H_2 \rightarrow He^0(n) + H_2{}^+(1s\sigma_g) \rightarrow H^+ + H^0(1s) \quad [H_2^+ \text{ground-state dissociation (GSD)}] \tag{2}$$

$$He^+ + H_2 \rightarrow He^0(n) + 2H^+ + e \quad \text{[transfer ionization (TI)]} \tag{3}$$

$$He^+ + H_2 \rightarrow He^0(n) + H_2{}^{+*} \rightarrow H^+ + H^0 \quad \text{[transfer excitation (TE)]} \tag{4}$$

In channel (4), the excitation transferred to the $H_2{}^+$ results in the dissociation of the molecular ion. In particular, we focus on the n-state-selective electron capture to different states of the projectile while the ionic target remains in the $1s\sigma_g$ state [reaction (1)]. From the measured distributions for the recoil momentum vector $\mathbf{p}$, we can obtain: (a) the n-state-selective single capture cross sections (via the parallel component of $\mathbf{p}$ with respect to the beam direction, i.e., p_l) and (b) the transverse momentum p_t distribution, which provides information on the angular scattering suffered by the projectile throughout the collision.

The paper is organized as follows: In Sec. II, we briefly summarize the experimental setup. Section III provides a brief description of the CTMC model employed to theoretically analyze the experimental data. In Sec. IV, we present and discuss the obtained results, and finally, in Sec. V, we draw our conclusions.

II. EXPERIMENT

The measurements have been performed with the COLTRIMS apparatus installed at the 300-kV Cockroft-Walton accelerator at the Centro Atómico Bariloche. A $^4He^+$ beam with energies from 25 to 200 keV collided with a molecular H_2 target, and the recoil-ion momentum of the fragment ionic molecules has been measured in coincidence with emerging neutral projectiles. Details of the experimental

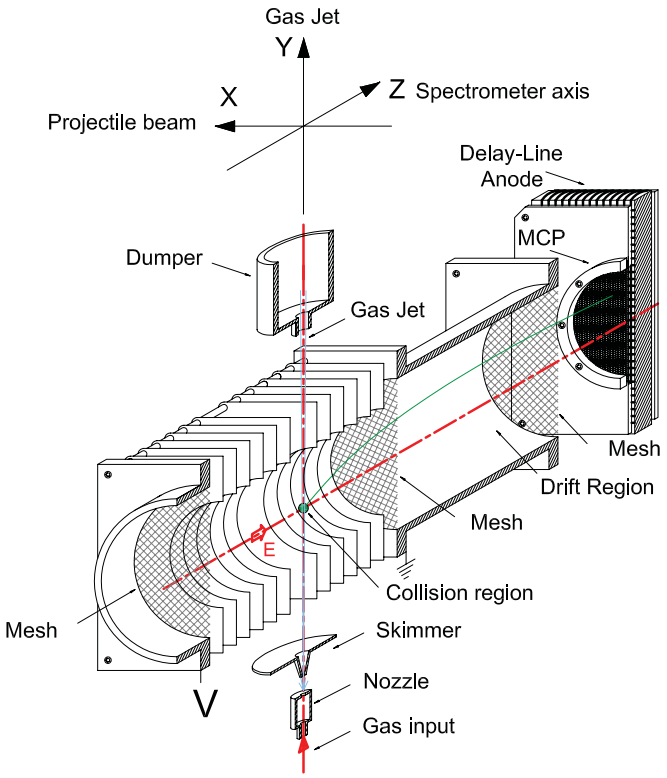

FIG. 1. (Color online) A schematic of the spectrometer setup half cut away through the symmetry plane. Also shown are the coordinate axes used: ion projectile beam along the x direction, gas jet along the y axis, and electric extraction field along the z axis.

configuration and methods used to process the measured data were described in Refs. [37,38]. Briefly, a continuous beam of $^4He^+$, magnetically selected, is delivered by the accelerator and is guided to the collision chamber. Before entering the collision chamber, the projectile beam is collimated by a pair of four adjustable slits producing a spot of approximately 0.4×0.6 mm^2 at the target position. The spectrometer is depicted in Fig. 1 together with the coordinate system used for the present measurements. The ion beam propagates along the x direction, the target gas jet is in the y direction, and the spectrometer axis is along the z direction. The projectiles cross the target jet at the collision region located inside the spectrometer. A homogeneous electrostatic field, along the z axis, extracts the recoil ions produced and projects them onto a position- and time-sensitive detector with a delay-line anode. The acceleration region in the spectrometer is followed by a field-free drift region that results in a time-focusing operation. The electric fields used for the present measurements were in the range from 2 to 10 V/cm. The target is supplied by a single-stage supersonic jet produced by an adiabatic expansion of H_2. The configuration of the target system consists of a 30-μm diameter nozzle followed by a skimmer (with an opening of 0.3-mm diameter) at a distance of 13 mm. The target system is differentially pumped with a diffusion pump. With a driving pressure of typically 2 bar, we achieve an estimated target density of 5×10^{11} molecules/cm^3 and a working pressure in the collision chamber of about 2×10^{-7} Torr. At the collision region, the gas jet has an estimated cross section of 1.2-mm diameter. The projectiles leaving the collision

chamber are separated into their different charge states by means of an electrostatic deflector. The selected projectiles hit a channeltron detector that provides the timing signal used for the measurement of the time of flight of the recoil ions and provides the coincidence condition for the desired collision process to be studied. From measurements of the hit position of the recoil ions on the position-sensitive detector and their time of flight, the three components of the initial momentum of the particles can be found from the ion trajectories inside the spectrometer as described elsewhere [37].

An important issue to be taken into consideration for recoil-ion spectroscopy is the initial random momentum of the target molecules. For the present case of a H_2 target, we provide estimates expressed in the following figures. After adiabatic expansion, the H_2 molecules, starting at room temperature, have a directed movement along the y axis of $p_y = 5.0$ a.u. that result from the terminal speed of the expanded gas. A random movement of the molecules originated on the left over temperature is overlapped to this terminal momentum. Using the speed ratio S for H_2 [39], we can perform a rough estimate of the temperature of the molecular beam to reach 4 K. This effect adds a mean-momentum spread of $\Delta p_y = \pm 0.24$ a.u. Along the x and z axes, the spread in momentum is described by the geometry of the gas jet. In the direction of the projectile beam, we estimate a spread for $p_x = \pm\ 0.06$ a.u., and in the perpendicular, we estimate a spread for $p_z = \pm\ 0.03$ a.u.

III. THEORETICAL MODEL

The present data have been contrasted to the theoretical results obtained by means of the CTMC method. This method has been extensively described in previous papers for ion-atom collisions [40–43]. Papers concerning molecular targets with the CTMC method are scarcer [29,44,45] due to the increasing complexity in the description of the initial target.

In this paper, we use the CTMC method presented by Wood and Olson to study double-electron removal in collisions involving highly charged ions and H_2 [46], which we adapt to study single-electron capture. Hamilton's equations are numerically solved by means of a fourth-order Runge-Kutta integration method with an adaptive step size. The interactions among particles are represented by Coulomb interactions,

$$V(r_{ij}) = \frac{Z_i Z_j}{r_{ij}}. \tag{5}$$

As each trajectory is initialized, the initial state of the molecular target is described by two independent hydrogen atoms held together by a Morse potential,

$$V_m(R) = D_e(1 - e^{-\beta_e(R-r_e)})^2, \tag{6}$$

where D_e is the dissociation energy, R is the separation of the atomic centers, r_e is the separation defined such that $V_m(r_e)$ is minimum, and β_e is the curvature parameter of the potential. The values for the parameters in V_m are determined from spectroscopic data [47], and for H_2, read $D_e = 4.75$ eV, $r_e = 1.4$, and $\beta_e = 0.73$ a.u.

The electron-electron and the electron-other-target-nucleus interactions are neglected at the early stages of the trajectory to avoid classical instability. The initial position and momentum of the electron regarding its parent nucleus are determined according to the hydrogenic microcanonical distribution. Additional random quantities are generated for the momenta of the nuclei as well as the separation distance of the nuclei about the vibrational ground state centered about the minimum of the Morse potential ($r_e = 1.4$ a.u.). In our treatment, the center of mass of the target is considered to be frozen. Thus, the momentum of each nucleus is such that the total momentum of the molecule is zero,

$$p_H = \pm\frac{P_{c.m.}}{2}, \tag{7}$$

Here, $P_{c.m.}$ is the momentum of the center of mass of the system given by

$$P_{c.m.} = \sqrt{2\mu[E_v - V_m(R)]}, \tag{8}$$

where μ is the reduced mass of the two atoms and E_v is the vibrational ground-state energy. The angle defining the intermolecular axis is randomly oriented, leading to a nonoriented target.

In this dynamical model, if an electron reaches the continuum with respect to its parent nucleus, the electron-electron and electron-nucleus interactions are turned on smoothly in the Hamiltonian. We used a switching function defined by $1 - e^{-\gamma(t-t_0)}$, where γ is a constant which we have set as 0.1 a.u. and t_0 is the time at which the electron reached the continuum with respect to its parent nucleus. Other γ values provided cross sections which differed in a few percent from those obtained with the chosen value. Furthermore, when one of the electrons is emitted from its parent nucleus, the remaining Coulomb interactions are smoothly switched on, and all five particles interact with each other.

An additional issue arises in the present case being the projectile of partially stripped nature. To represent the electron-projectile interaction, we have used the central potential model developed by Green *et al.* [48] from Hartree-Fock calculations and, later on, generalized by Garvey *et al.* [49]. To calculate the n-state-selective capture cross sections, we have used the model developed by Schultz *et al.* [50], which introduces an effective charge $q(U)$, which represents the charge seen by the captured electron according to its binding energy (see Fig. 2). A classical n value can then be inferred from the rearranged Bohr formula,

$$n_c = \frac{q(U)}{(2U)^{1/2}}, \tag{9}$$

where the relation between the effective charge and the binding energy U is provided by the Bohr orbit condition,

$$U(r) = -V_{\text{mod }el}(r)/2. \tag{10}$$

Such a procedure represents an imperfect but improved method to establish the correspondence of the classical final state and the most appropriate quantal state. These classical n_c values are then related to specific n levels according to the relationship derived by MacKellar and Becker [51],

$$\left[(n-1)\left(n-\tfrac{1}{2}\right)n\right]^{1/3} \leqslant n_c \leqslant \left[n\left(n+\tfrac{1}{2}\right)(n+1)\right]^{1/3}. \tag{11}$$

Finally, we point out that the number of capture events binned as going into $n = 1$ has been multiplied by a "blocking factor"

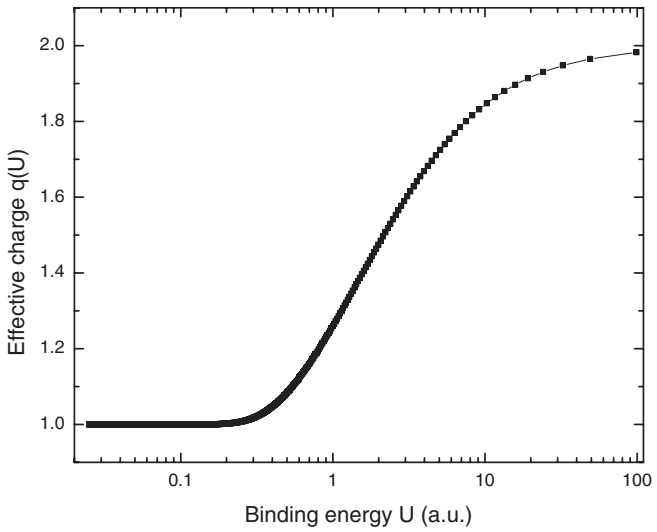

FIG. 2. Effective charge seen by the captured electron as a function of the binding energy as it results from the Bohr orbit model.

of 1/2 in order to compensate for the overestimation proper of our one-electron treatment, which does not naturally account for partially filled shells.

Before proceeding to the comparison with the present experimental data, we benchmark our CTMC model at the total cross-sectional level. In Fig. 3, our theoretical results for one-electron capture are contrasted with those published at different impact energies by several laboratories worldwide [19,23,52,53]. In Table I, we list the total cross sections that resulted. These cross sections involve contributions from the SC, GSD, TE, and TI channels. We observe that the CTMC total cross sections are in very good agreement with the data, in particular, in the energy range of 25–200 keV of our concern. In the following section, the experimental state-selective single

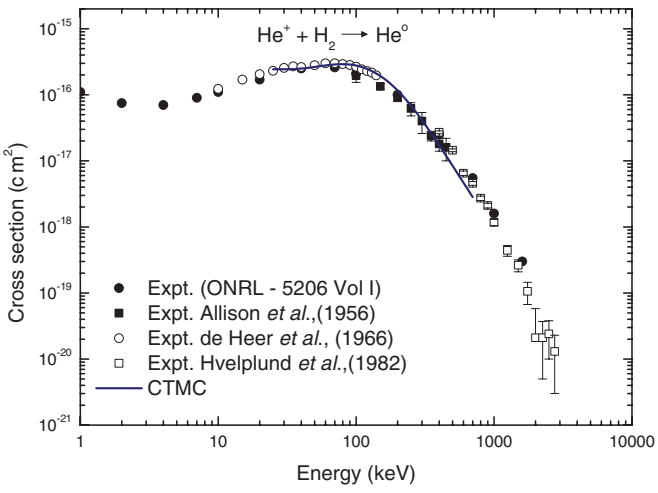

FIG. 3. (Color online) Total cross section for the process of charge exchange for $He^+ + H_2$ collisions in coincidence with emerging He^0 projectiles. Experimental data: filled circles, Oak Ridge National Laboratory (ORNL) data tables [53]; filled squares, Allison *et al.* [19]; open circles, de Heer *et al.* [52]; open squares, Hvelplund and Andersen [23]. Theory: solid line, present CTMC calculations.

TABLE I. CTMC total cross sections for the experimental collision energies explored in this paper: 25, 40, 50, 100, and 200 keV (in units of 10^{-16} cm^2).

Energy (keV)	Total cross sections CTMC
25	2.435
40	2.496
50	2.640
100	2.782
200	1.166

capture cross sections will be normalized with those provided by the CTMC model.

IV. RESULTS AND DISCUSSION

For an inelastic collision involving two bodies, as in the present case of charge exchange, it can be shown from energy and momentum conservations and in the case of small scattering angles and changes in projectile energy, that the longitudinal momentum p_l (which can be also termed p_x in view of the coordinate system shown in Fig. 1) and transverse momentum p_t (with respect to the direction of the incident projectile beam) acquired by the recoil ion, are independent. For a capture reaction, p_l and p_t are given (in atomic units) by

$$p_l = -\frac{Q}{v_p} - n_e \frac{v_p}{2}, \tag{12}$$

$$p_t = -P_P \theta_P. \tag{13}$$

Here, v_p, P_P, and θ_P are the projectile velocity, momentum, and scattering angle, respectively. n_e is the number of electrons transferred from the target to the projectile; for the present case, it is $n_e = 1$. Q gives the change in electronic energy of the reaction. It is obtained as the difference between the binding energies in the target and the projectile.

From Eq. (13), it can be seen that performing recoil-ion spectroscopy using energy and momentum conservation in a typical two-body collision provides an alternative route to gain insight on the angular distribution of the receding projectile.

The transverse momentum p_t for the recoil ion is given by

$$p_t = \sqrt{p_y^2 + p_z^2}. \tag{14}$$

For the reaction channel (1), SC, in Table II, we display the Q values for capture into the ground state and first excited states of the He projectile. For the binding energies of the He atom [54,55], when one electron is in the $n = 2$ level, we use a set of values that range from 3.37 to 4.77 eV for the four sublevels ($2\,^1P$, $2\,^3P$, $2\,^1S$, and $2\,^3S$). When $n = 3$, for the six sublevels (singlets and triplets S, P, and D), we use values from 1.50 eV to 1.87 V. For the H_2 molecule, the excitation from the ground state of the molecule, in the vibration state $v = 0$, to the ionic molecule involves a range of values from 15.43 to 18.08 eV [56]. This corresponds with the possibility of excitation into all vibrational states of the ground electronic state $X\,^2\Sigma_g^+$ ($1s\sigma_g$) of the H_2^+ ion. In Fig. 4, we display potential curves for the H_2 and H_2^+ to show the transitions involved. For the present collision system $He^+ + H_2$, as can be seen from Table II, a range of several closely lying Q

TABLE II. Q values for single-electron capture used. The binding energies are indicated in parentheses, in eV and are used for the transition from H_2 ($v = 0$) to H_2^+ ($v = 0$, most probable and threshold of dissociation).

Final state	Description state He	Q min (a.u.) (18.1-eV H_2)	Q med. (a.u.) (16.28-eV H_2)	Q max (a.u.) (15.4-eV H_2)
(1,1)	$1\,^1S$	0.24	0.31	0.34
(2,1)	$2\,^1S$	−0.52	−0.45	−0.42
	$2\,^1P$	−0.54	−0.48	−0.44
	$2\,^3S$	−0.49	−0.42	−0.39
	$2\,^3P$	−0.53	−0.47	−0.43
(3,1)	$3\,^1S$	−0.60	−0.54	−0.51
	$3\,^1P$	−0.61	−0.54	−0.51
	$3\,^1D$	−0.61	−0.54	−0.51
	$3\,^3S$	−0.60	−0.53	−0.50
	$3\,^3P$	−0.61	−0.54	−0.51
	$3\,^3D$	−0.61	−0.54	−0.51

values are possible. If we assume, for the present collision system, that the collision time (about 10^{-16} s) is fast enough that the transitions can be considered under the frame of the Franck-Condon principle (vibration time typically in 10^{-14} s). We use, as a value the energy necessary for creation of the ionic state, a value of 16.3 eV. Here, the ionic molecule H_2^+ emerges from the collision excited into some vibrational state $v > 0$.

In Fig. 5, we show a measured distribution of H_2^+ ions, in the detector plane, of typical collected data corresponding to SC. We observe, in general, as the figure displays for the particular case of 25-keV incident projectiles, two broad peaks that we associate with state-selective electron capture to different final states of the projectile. The highest peak corresponds to a single charge-exchange process in which the target is ionized and is left in the $^2\Sigma_g^+(1s\sigma_g)$ state, and the projectile captures the target electron in the $(n_1 = 1, n_2 = 1)$ $1\,^1S$ ground state. The lowest peak, on the other hand, is built upon the contributions of the electron capture to excited states of He. Those are indicated as $(n_1 = 1, n_2 = 2)$ (which comprise the contributions arising from the $2\,^3S$, $2\,^1S$, $2\,^3P$, and $2\,^1P$ states), and $(n_1 = 1, n_2 = 3)$ (which comprise the contributions from $3\,^3S$, $3\,^1S$, $3\,^1P$, $3\,^3P$, $3\,^3D$, and $3\,^1D$). The broad strip of events displayed in Fig. 5 that runs along the x axis represents a background signal due to ions present in the residual gas in the collision chamber.

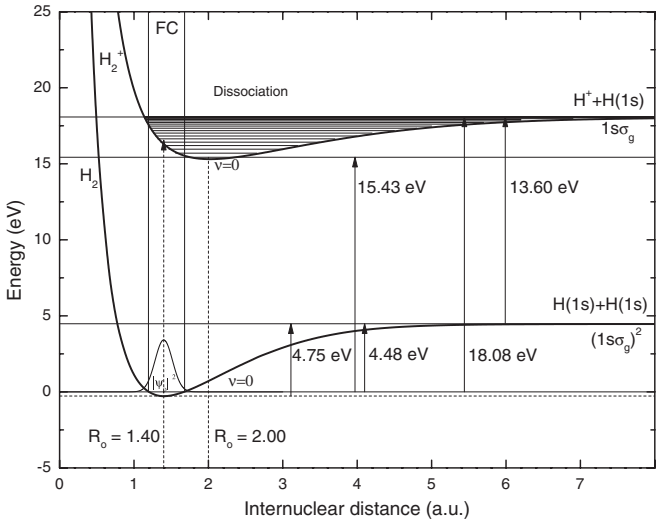

FIG. 4. Potential-energy curves for the electronic ground states of H_2 and H_2^+ (according to Ref. [56]).

A. Longitudinal momentum and state-selective electron capture

In Figs. 6(a)–6(e), we show the p_x distribution of the H_2^+ ions which correspond to SC at impact energies of 6.25, 10, 12.5, 25, and 50 keV/amu. The background events, due to interactions with the uniformly distributed gas in the collision chamber and from random coincidences, were subtracted following the procedure described in Ref. [37]. We see that all the distributions in the figures show a two-peak structure as

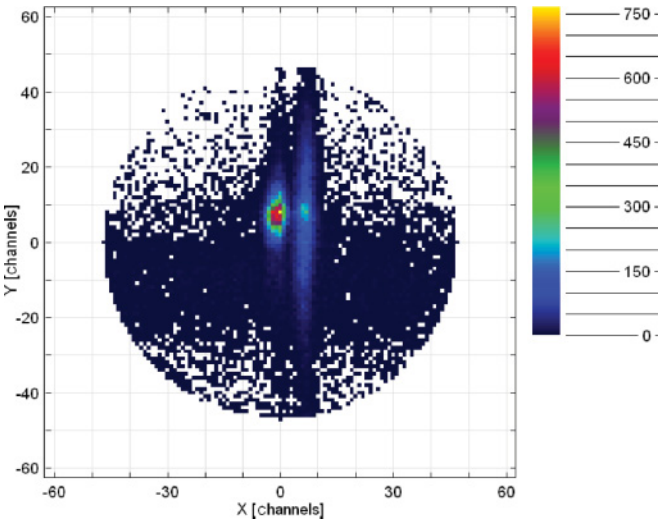

FIG. 5. (Color online) Image from the position-sensitive detector in the x,y plane of H_2^+ recoil ions in coincidence with He^0 emerging projectiles, corresponding to a single capture process. Collision of 25 keV $^4He^+$ incident on H_2, with an electric extraction field of 10 V/cm. Ions created in the jet result in the well-localized spots. The broad- and low-intensity horizontal traces (along the x direction) result in a background from the residual gas in the collision chamber.

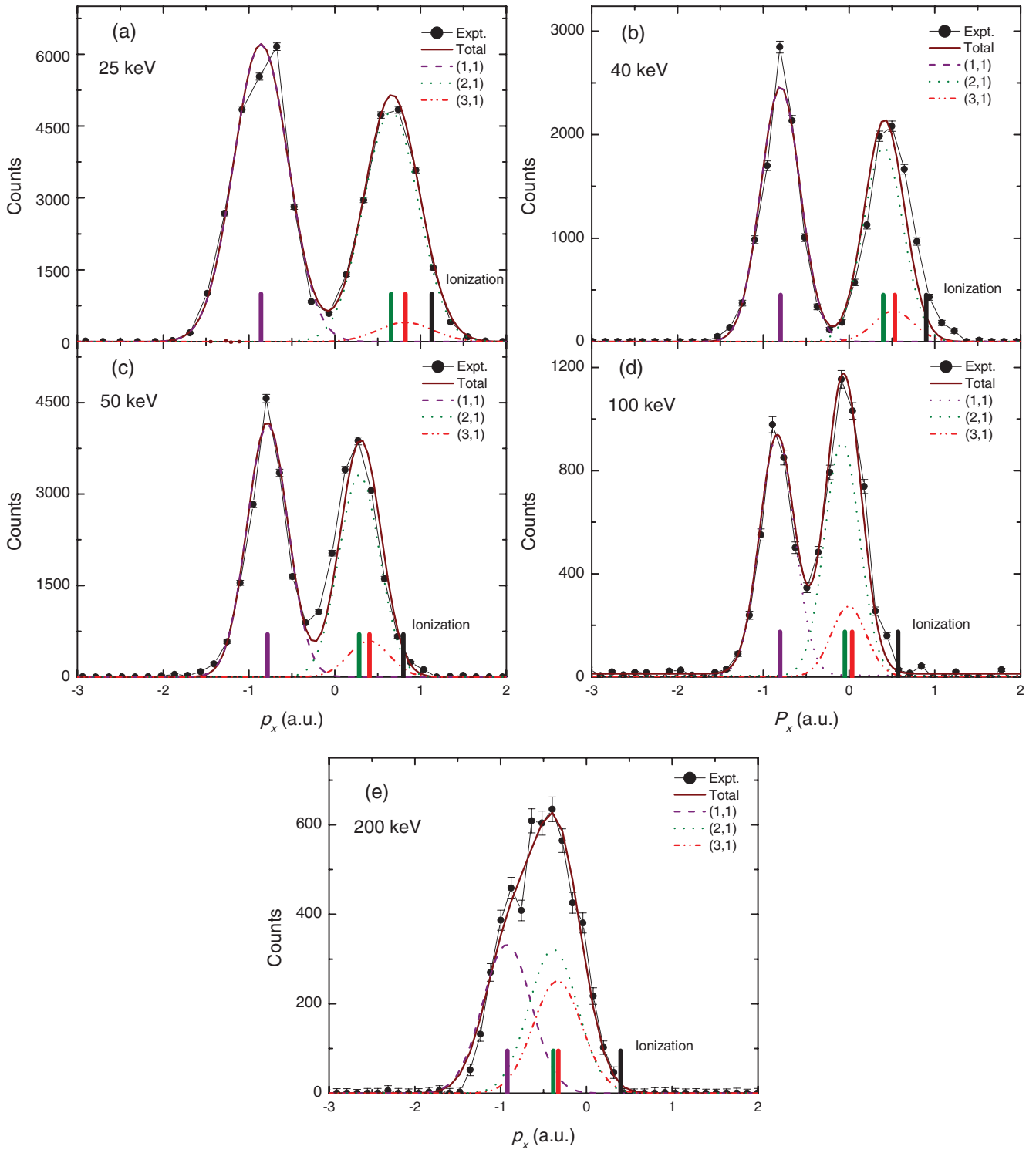

FIG. 6. (Color online) Experimental longitudinal momentum distribution of H_2^+ recoil ions integrated over p_y and p_z for 25-, 40-, 50-, 100-, and 200-keV incident He^+ projectiles. Also displayed are the fittings of the experimental data with three Gaussian peaks. The bars indicate the theoretical position of the peaks. The ionization bar indicates the expected place where contamination from the incident projectile beam may contribute.

previously mentioned with regard to Fig. 5. The momentum distributions reflect different inelastic processes as described by Eq. (12). Knowing the Q values involved, given in Table II from theoretical structure information for He and H_2 collision partners [54–56], we can identify the processes involved. The left peak is associated with electron capture to the ($n_1 = 1$, $n_2 = 1$) $1\ ^1S$ ground state of He, while the right one and more broader one is associated with electron capture to several

TABLE III. Theoretical longitudinal momentum p_l for state-selective electron capture into (1,1), (2,1), and (3,1) states. Also indicated are the values corresponding to the maximum of ionization (where low-energy electrons are emitted).

	Energy (keV/amu)				
Final state	6.26	10	12.5	25	50
(1,1)	−0.86	−0.80	−0.79	−0.81	−0.92
(2,1)	0.66	0.40	0.29	−0.05	−0.39
(3,1)	0.82	0.53	0.41	0.04	−0.33
Ionization	1.13	0.90	0.80	0.57	0.40

excited states of the projectile while the target ion H_2^+ remains in the ground state. At the lower impact energies of 6.2, 10, and 12.5 keV/amu, we note that the peaks for the ground state and excited states are well enough separated to be resolved. At the larger impact energies of 25 and 50 keV/amu, these structures overlap, and the separation of the n-state-selective SC cross sections becomes more involved.

The experimental longitudinal momentum distributions p_x have been fitted using Gaussian shaped peaks, which are also displayed in Fig. 6. The experimental distributions have been normalized to the theoretical CTMC results for total cross sections for the SC channel. From these fits, the state-selective cross sections are obtained and are listed in Table III. The fit of the single peak associated with the $1\,^1S$ state of He presents no problem. But, the second peak, attributed to the excited states, requires some explanations. In this case, as can be seen from the Q values in Table II, several closely spaced levels are present that can hardly be resolved with our spectrometer. We assumed a mean-Q value for the $n = 2$ group and did the same for the $n = 3$ group. These mean values are close to the corresponding Q values that may result for the ^1S energy levels of He. Even though the resulting Q values for $n = 2$ and $n = 3$ are quite close, they were explicitly considered in our fitting procedure. The location of the states corresponding to $n = 1$ and (the pseudomean states) 2 and 3 are shown as bars in Fig. 6. Also, a bar indicates the location where the ionization continuum may present the maximum yield [57]. No events from ionization are expected to be observed because they are excluded by the coincidence condition on the measurement.

The general trend that can be inferred from Fig. 6 and Table IV is that of a larger probability of capture to ($n_1 = 1$, $n_2 = 1$) at the lower-impact energies compared to the combined

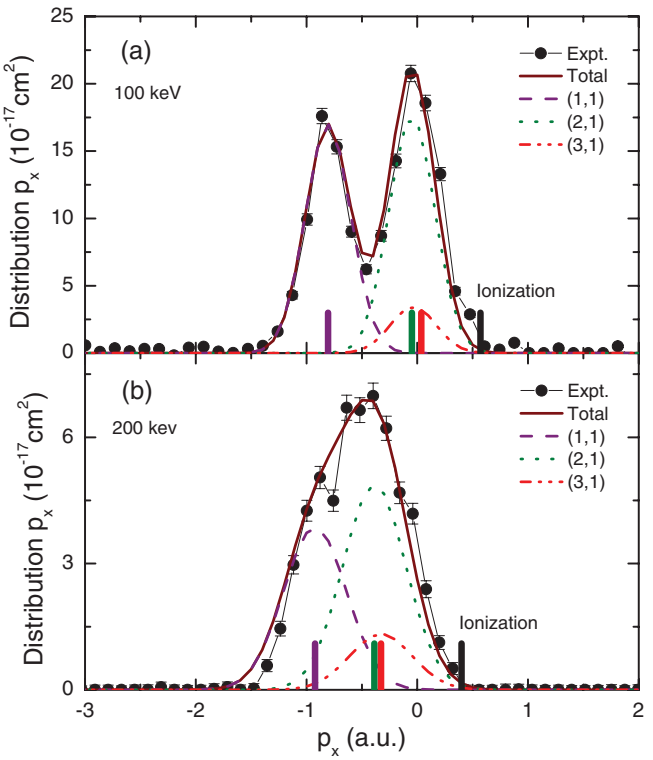

FIG. 7. (Color online) Experimental longitudinal momentum distribution for two projectile energies (a) 100 and (b) 200 keV. Lines, results obtained from the present CTMC theory.

($n_1 = 2, n_2 = 1$) and ($n_1 = 3, n_2 = 1$) channels, a situation that reverses as the impact energy increases. At 25 keV/amu, the ($n_1 = 2, n_2 = 1$) and ($n_1 = 3, n_2 = 1$) channels clearly dominate over ($n_1 = 1, n_2 = 1$). It is well known from charge-exchange reactions on atomic targets at intermediate impact energies, that the n distributions tend to increase their width and even shift the positions of their maxima to larger n values as the impact energy is increased [58,59]. The present results suggest a similar trend for the molecular case explored.

In Figs. 7(a) and 7(b), we contrast our experimental and theoretical longitudinal momentum distributions at 25 and 50 keV/amu. We have convoluted our n-state-selective SC CTMC cross sections using Gaussian functions which mimic the resolution of the spectrometer. The theoretical data are in close agreement with the measured data.

TABLE IV. Experimental state-selective cross sections for single-electron capture for $He^+ + H_2 \rightarrow He^0 + H_2^+$ collisions in units of 10^{-16} cm^2. In parentheses are the values in percentages.

	Energy (keV/amu)				
Final state	6.25	10	12.5	25	50
(1,1)	0.99 ± 0.10 (54.4)	1.01 ± 0.15 (53.1)	1.05 ± 0.16 (51.4)	0.92 ± 0.19 (44.0)	0.27 ± 0.05 (37.7)
(2,1)	0.77 ± 0.08 (42.1)	0.77 ± 0.12 (40.5)	0.84 ± 0.13 (41.2)	0.90 ± 0.18 (43.0)	0.27 ± 0.12 (37.7)
(3,1)	0.06 ± 0.03 (3.5)	0.12 ± 0.06 (6.4)	0.15 ± 0.08 (7.4)	0.27 ± 0.14 (13.0)	0.18 ± 0.09 (24.6)

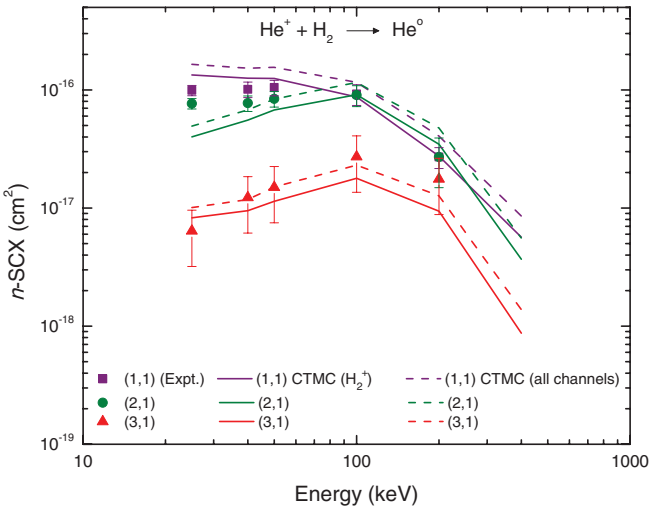

FIG. 8. (Color online) State-selective cross sections for single-electron capture for $He^+ + H_2 \rightarrow He^0 + H_2^+$ collisions. Filled symbols, experimental results of this paper; full lines, present CTMC calculations for only a SC process; dotted lines, CTMC result for all charge-exchange processes (SC, GSD, TE, and TI).

In order to provide a more exhaustive analysis, in Fig. 8, the experimental and theoretical n-state-selective cross sections are compared. Good overall agreement is obtained, especially in describing the inversion of the dominant reaction channels at about 100 keV. Nevertheless, we notice that, at low-impact energies, the CTMC results tend to underestimate the contribution arising from the $(n_1 = 2, n_2 = 1)$ channel. This could be probably related to our one-electron model for the impinging projectile. It could be possible that the introduction of the simple blocking factor to account for the partially filled shell cannot compensate for the lack of a proper description of the electron-electron interaction.

In addition, we note that our theoretical state-selective one-electron capture cross sections, including all four possible channels, show an energy dependence which closely follows that shown by channel (1) itself. This suggests that by experimentally accessing channel (1), it would be possible to estimate the relative population of the different levels for the single capture process.

B. Transversal momentum components p_y, p_z

In Fig. 9, we show the transversal momentum component distributions along the y and z axes. The figure displays the total- and state-selective distributions for the impact energy 10 keV/amu. The background has been subtracted following the same procedure used for the p_x distributions.

Due to the cylindrical symmetry of the collision process, it was expected that both distributions p_y and p_z should display equivalent shapes for the two perpendicular components. Nevertheless, in this case, we can see a marked difference in that the p_y distributions are wider than the p_z distributions. This difference we can only attribute to the thermal random momentum present in the target atoms. Along the y direction, the gas jet has a residual temperature after adiabatic expansion to which is also added the detector spatial resolution and the target size. On the contrary, along

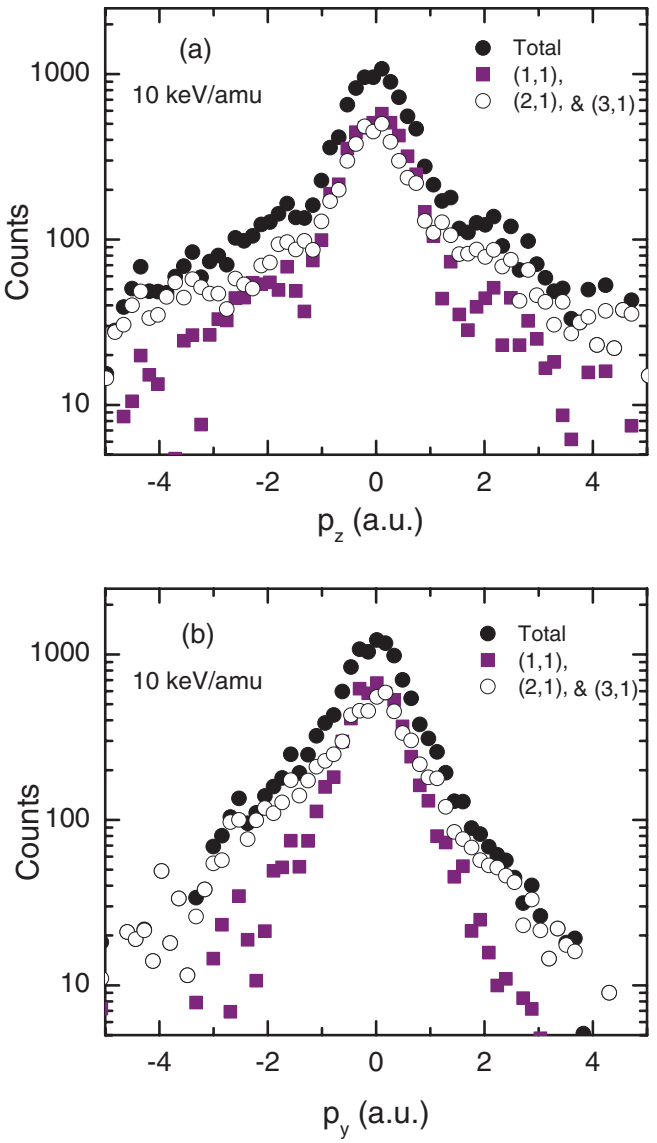

FIG. 9. (Color online) Projection distributions of transversal momentum along the z (a) and y axes (b) for 10-keV/amu incident He^+ projectiles. The figure displays the total distribution for SC and the components corresponding to SC for the ground and excited states of He.

the z direction, the target molecules due to the geometrical cooling, the gas jet has a significantly smaller initial random momentum component. Additionally, from the time focusing geometry of the spectrometer, the p_z distribution should not be affected by the target size. Hence, we trust that the p_z distributions reflect mainly the momentum transferred in the collisions.

In Fig. 10, we show the experimental results for the p_z distributions along with the classical trajectory Monte Carlo method. We find that the theory yields good agreement for the total distributions in the central part of the peak, but large differences are visible in the tails of the distributions. The data in Fig. 10 show that events corresponding to larger scattering angles provide an important contribution to the capture process. The experimental data even show an

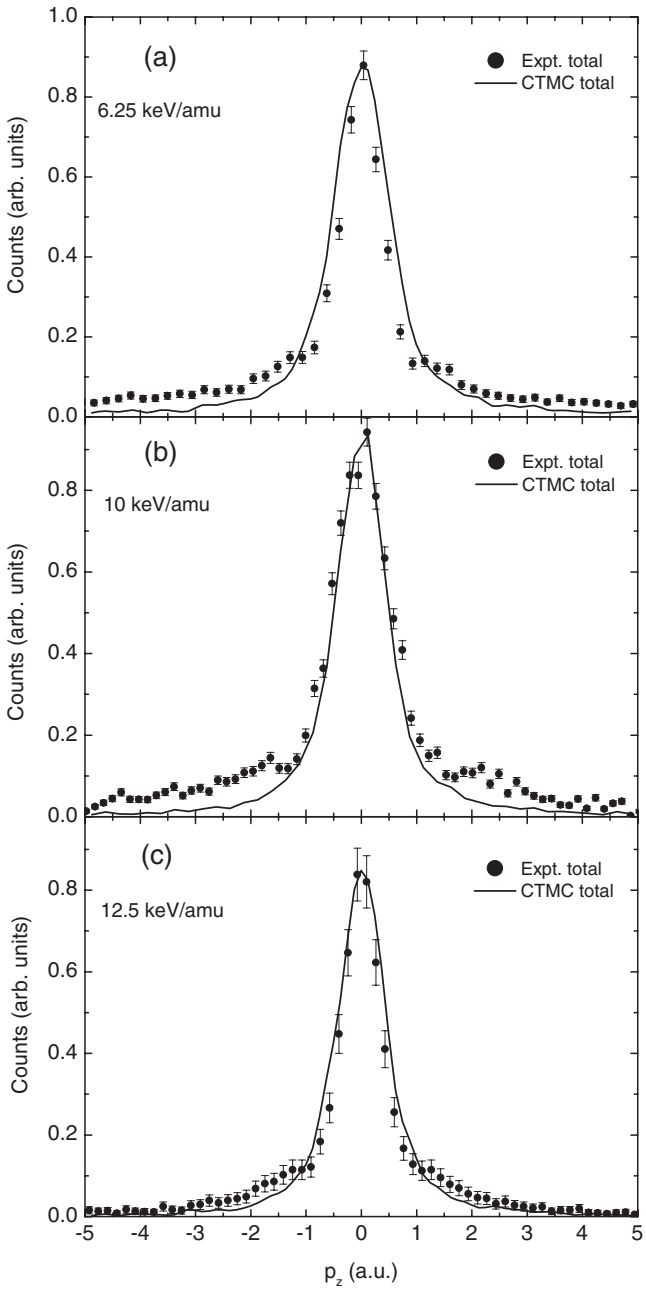

FIG. 10. Total experimental and CTMC momentum projections along the z axis for (a) 6.25-, (b) 10-, and (c) 12.5-keV/amu incident He^+ projectiles.

oscillatory structure that is not described by the CTMC model and that is discussed in the following section.

C. Transversal momentum p_t

In the case of the measured p_y and p_z distributions, due to the fact that they are affected along one direction by a thermal component, we cannot directly apply Eq. (14) to find the transversal momentum distribution originated from the collision. The target we used had no sufficient cooling as previously discussed in the Experimental section. However, the thermal motion mainly affects the target motion in the y-axis direction with an estimated initial momentum spread of $\Delta p_y = \pm 0.24$ a.u. In the z axis, on the other hand, the thermal motion effects are expected to be very small (only a small spread resulting from the beam and jet geometry, which may contribute with an estimated $\Delta p_z = \pm 0.03$ a.u., a value much smaller than the thermal spread). Under these conditions, we assume that we can extract the transversal momentum distribution from our measured p_z distributions. The arguments for the procedure that we use are the following. The probability (or else, cross section) for a collisionally originated momentum may be given by the distribution,

$$f_c(\mathbf{p}_c) = f_c\left(\sqrt{p_{yc}^2 + p_{zc}^2}\right), \tag{15}$$

where $\mathbf{p}_c$ is the collisionally originated momentum and expression (15) reflects the cylindrical collision symmetry. For the thermal distribution, we assume an expression,

$$f_T(\mathbf{p}_T) = f_T(p_{yT})\delta(p_{zT}), \tag{16}$$

where $\mathbf{p}_T$ is the thermal momentum contribution initially present in the target particle, and δ is the Delta function. Taking into account the relation $\mathbf{p} = \mathbf{p}_c + \mathbf{p}_T$, the combined distribution that is measured reads

$$f_{cT}(\mathbf{p}) = \int_{-\infty}^{\infty} f_c\left(\sqrt{p_{zc}^2 + u^2}\right) f_T(p_{yT} - u)du. \tag{17}$$

Equation (17) results as a convolution of f_T over f_c, where $\mathbf{p}$ is the measured momentum. From Eq. (17), we obtain, for the projected momentum distribution P_z along the z axis,

$$P_z(p_z) = \int_{-\infty}^{\infty} f_{cT}(p_y, p_z)dp_y = \int_{-\infty}^{\infty} f_c\left(\sqrt{p_z^2 + u^2}\right)du, \tag{18}$$

where we used the fact that the probability distribution f_T must be normalized to 1. Equation (18) shows that, under the present assumptions, the projection of the measured combined momentum distribution along the z axis yields the same result as projecting the collisional distribution along the same axis. Here, in Eqs. (15)–(18), f_c and $\mathbf{p}_c$ are the transversal momentum distribution and the transversal momentum ($\mathbf{p}_t$), respectively, which we seek. Due to the unequal initial momentum spread of the target molecules, we see that, only from a projection along the z axis, is it possible to extract the original circular symmetric transversal momentum distribution. The same argument cannot be applied for the y-axis projection for which an expression different from Eq. (18) results.

We use the result of Eq. (18), starting from the measured distributions for p_z, to find the p_t distributions. In this sense, Eq. (18) is equivalent to an Abel transform for which the inversion or resolvent expression is known [60], which we used to extract the p_t distribution. We directly applied the inversion formula that consists of the calculation of an integral and a derivative. In order to reduce random-noise-related effects that can adversely act on a derivative calculation, the p_z experimental spectra have been smoothed before applying the inversion formula. As a control check for the numerical calculation, after obtaining the transversal distributions, we backprojected our distribution on the z axis obtaining excellent agreement with the original measured projection. This gives us

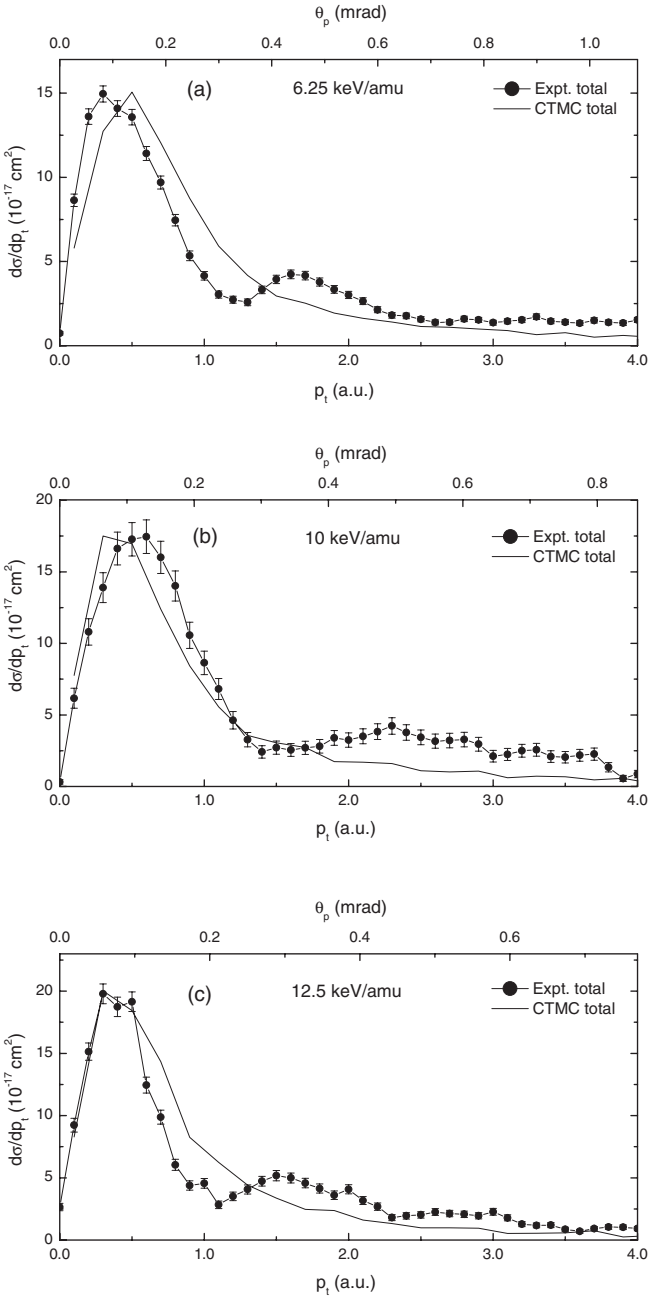

FIG. 11. Total experimental and CTMC transversal momentum distributions as a function of p_t and projectile scattering angle θ_P. (a) 6.25-, (b) 10-, and (c) 12.5-keV/amu incident He^+ projectiles. Experimental data have been normalized with CTMC results.

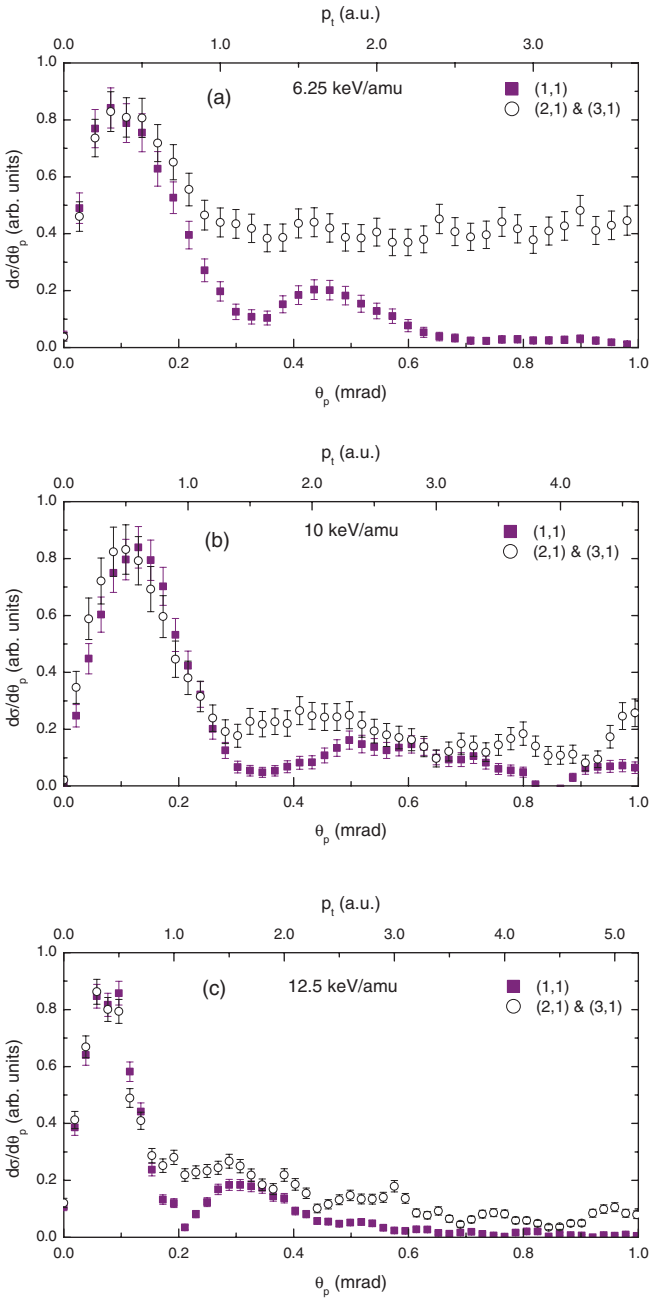

FIG. 12. (Color online) Experimental projectile scattering angle distributions for ground- and excited-state SCs. For (a) 6.25-, (b) 10-, and (c) 12.5-keV/amu incident He^+ projectiles.

confidence that no artificial deformations of the distributions have been introduced by the numerical procedure used.

In Figs. 11(a)–11(c), we show differential cross sections in transverse momentum for 6.25-, 10-, and 12.5-keV/amu impact energies. We additionally show the distributions as a function of the scattering angle by means of Eq. (13). We clearly observe, from the present data and CTMC results, that most of the contribution corresponds to small scattering angles with a maximum present around 0.1–0.2 mrad. In addition, we note that the present data show, in all cases, an oscillatory structure which is not reproduced by the CTMC results. The oscillatory structure observed is also present in the projected distributions (nearly raw data except for the background subtraction) as can be seen in Figs. 9 and 10. In Fig. 12, we show the separate contributions to the experimental transverse momentum distributions of the (1,1), (2,1), and (3,1) channels. We observe that the oscillatory structure is much more pronounced for the (1,1) channel. A similar oscillatory behavior has been reported by the Frankfurt group in their pioneering COLTRIMS works for single-electron capture in ion-atom collisions and was explained in terms of K-K resonances [10,61,62]. Contrary to that case, the present system is nonquasiresonant [63,64], and other possible

sources of oscillatory patterns in the projectile scattering angle (or p_t) distributions should be invoked. One type of oscillatory structure results from the interference of scattering amplitudes corresponding to different reaction pathways. Landau [65], Zener [66], and Demkov [67] models have been used to model this phenomenon. Another type of oscillatory structure arises from quantum or classical effects involving the attractive and repulsive parts of the potential surfaces relevant to the collision, such as diffraction or rainbow scattering [68,69]. A more exhaustive exploration is needed at this point before a definitive assertion can be made on the physical origin of the oscillatory structures seen in Figs. 11 and 12.

V. CONCLUSIONS

In this paper, state-selective single-electron capture in collisions of He^+ with H_2 molecules has been investigated using the COLTRIMS technique. The energy range considered was that proper of the Kevatron accelerator (6.25–50 keV/amu).

The state-selective capture cross sections have been obtained from the longitudinal H_2^+ recoil-ion momentum distributions and have been contrasted against CTMC simulations finding good overall agreement. The resolution of our spectrometer allowed a clear separation of contributions for the (1,1), (2,1), and (3,1) states for impact energies below 25 keV/amu. For impact energies larger than about 50 keV/amu, the longitudinal recoil momentum distributions overlap in such an extent that the separation of the n-state-selective SC cross sections would become unfeasible for our present setup. In addition, we note that the present theoretical results for the state-selective cross sections suggest that the relative population of the (1,1), (2,1), and (3,1) states in single-electron capture can be estimated from the present experimental data, which only consider one of the four possible channels contributing to the process.

We have performed an inversion procedure over the p_z distribution, which in principle and due to geometrical cooling, is not affected by the thermal motion. This procedure allowed us to gain access to the p_t distribution. Both experimental and theoretical distributions showed that the transverse momentum distribution peak at scattering angles between 0.1 and 0.2 mrad for the impact energies under consideration. In addition, we found an oscillatory structure that can be mainly traced to charge exchange for the (1,1) state. This structure is not reproduced by the CTMC results, and further work is needed before a definite assessment can be made on its origin. More work is currently under way to further investigate this particular issue.

Concerning the potential application of the present paper (and future related papers), we note that He^{2+} is the most abundant solar wind ion besides H^+, and planetary atmospheres are constituted in an 80%–95% of H_2 [33]. It is then expected that single charge-exchange processes between He^{2+} and planetary atmospheres could lead to a considerable amount of He^+ ions which could undergo charge-exchange collisions as well. The latter would mainly depend on the thickness (or extension) of the gaseous environment.

ACKNOWLEDGMENTS

Work at Centro Atómico Bariloche was supported by CNEA (Argentina). Work at UNS was supported by Grants No. PGI 24/F049 of UNS, No. PICT 2007-00887 of ANPCyT, and No. PIP 112-200801-02760 of CONICET (Argentina).

[1] B. Gervais, M. Beuve, G. H. Olivera, and M. E. Galassi, Radiat. Phys. Chem. **75**, 493 (2006).
[2] T. E. Cravens, Science **296**, 1042 (2002).
[3] S. Otranto, R. E. Olson, and P. Beiersdorfer, J. Phys. B **40**, 1755 (2007).
[4] R. C. Isler, Plasma Phys. Controlled Fusion **36**, 171 (1994).
[5] www.iter.org.
[6] R. Moshammer, M. Unverzagt, W. Schmitt, J. Ullrich, and H. Schmidt-Böcking, Nucl. Instrum. Methods Phys. Res. B **108**, 425 (1996).
[7] R. Dörner, V. Mergel, O. Jagutzki, L. Spielberger, J. Ullrich, R. Moshammer, and H. Schmidt-Böcking, Phys. Rep. **330**, 95 (2000).
[8] J. Ullrich, R. Moshammer, A. Dorn, R. Dörner, L. P. Schmidt, and H. Schmidt-Böcking, Rep. Prog. Phys. **66**, 1463 (2003).
[9] W. Wu, K. L. Wong, C. L. Cocke, J. P. Giese, and E. C. Montenegro, Phys. Rev. A **51**, 3718 (1995).
[10] V. Mergel *et al.*, Nucl. Instrum. Methods Phys. Res. B **98**, 593 (1995).
[11] R. Dörner *et al.*, Phys. Rev. A **57**, 1074 (1998).
[12] A. Dorn, A. Kheifets, C. D. Schröter, B. Najjari, C. Höhr, R. Moshammer, and J. Ullrich, Phys. Rev. Lett. **86**, 3755 (2001).
[13] D. Fischer *et al.*, Phys. Rev. Lett. **90**, 243201 (2003).
[14] M. van der Poel, C. V. Nielsen, M. A. Gearba, and N. Andersen, Phys. Rev. Lett. **87**, 123201 (2001).
[15] J. W. Turkstra, R. Hoekstra, S. Knoop, D. Meyer, R. Morgenstern, and R. E. Olson, Phys. Rev. Lett. **87**, 123202 (2001).
[16] X. Flechard, H. Nguyen, E. Wells, I. Ben-Itzhak, and B. D. DePaola, Phys. Rev. Lett. **87**, 123203 (2001).
[17] V. G. Hasan, S. Knoop, R. Morgenstern, and R. Hoekstra, J. Phys: Conf. Ser. **58**, 199 (2007).
[18] S. Otranto, R. E. Olson, V. G. Hasan, and R. Hoekstra, in *n-Selective Single Capture Following Xe^{18+} and Xe^{54+} Impact on Na(3s) and $Na^*(3p)$*, edited by F. D. McDaniel and B. L. Doyle, AIP Conf. Proc. No. 1336 (AIP, New York, 2011), p. 158.
[19] S. K. Allison, J. Cuevas, and P. G. Murphy, Phys. Rev. **102**, 1041 (1956).
[20] C. F. Barnett and P. M. Stier, Phys. Rev. **109**, 385 (1958).
[21] L. I. Pivovar, V. M. Tuvaev, and M. T. Novikov, Sov. Phys. JETP **14**, 20 (1962).
[22] H. B. Gilbody, J. B. Hasted, J. V. Ireland, A. R. Lee, E. W. Thomas, and A. S. Whiteman, Proc. R. Soc. London, Ser. A **274**, 40 (1963).
[23] P. Hvelplund and A. Andersen, Phys. Scr. **26**, 375 (1982).

[24] W. L. Nutt, R. W. McCullough, K. Brady, M. B. Shah, and H. B. Gilbody, J. Phys. B **11**, 1457 (1978).
[25] R. Hoekstra, A. R. Schlatmann, F. J. de Heer, and R. Morgenstern, J. Phys. B **22**, L603 (1989).
[26] G. J. Frieling, R. Hoekstra, E. Smulders, W. J. Dickson, A. N. Zinoviev, S. J. Kuppens, and F. J. de Heer, J. Phys. B **25**, 1245 (1992).
[27] R. Hoekstra, H. O. Folkerts, J. P. Beijers, R. Morgenstern, and F. J. de Heer, J. Phys. B **27**, 2021 (1994).
[28] D. Bordenave-Montesquieu and R. Dagnac, J. Phys. B **27**, 543 (1994).
[29] L. Meng, R. E. Olson, H. O. Folkerts, and R. Hoekstra, J. Phys. B **27**, 2269 (1994).
[30] D. M. Kearns, R. W. McCullough, and H. B. Gilbody, Int. J. Mol. Sci. **3**, 162 (2002).
[31] T. Kusakabe, Y. Miyamoto, M. Kimura, and H. Tawara, Phys. Rev. A **73**, 022706 (2006).
[32] S. Figueira da Silva, H. P. Winter, and F. Aumayr, Phys. Rev. A **75**, 042706 (2007).
[33] R. J. Mawhorter, J. B. Greenwood, A. Chutjian, T. Haley, C. D. Mitescu, and J. Simcic, Phys. Rev. A **84**, 052714 (2011).
[34] E. Pollak and Y. Hahn, Adv. At. Mol Phys. **22**, 243 (1986).
[35] M. G. Suraud, R. Hoekstra, F. J. de Heer, J. J. Bonnet, and R. Morgenstern, J. Phys. B **24**, 2543 (1991).
[36] G. Lubinski, Z. Juhasz, R. Morgenstern, and R. Hoesktra, J. Phys. B **33**, 5275 (2000).
[37] M. Alessi, D. Fregenal, and P. Focke, Nucl. Instrum. Methods Phys. Res. B **269**, 484 (2011).
[38] M. Alessi, S. Otranto, and P. Focke, Phys. Rev. A **83**, 014701 (2011).
[39] D. R. Miller, in *Atomic and Molecular Beam Methods*, edited by G. Scoles, D. Bassi, U. Buck, and D. Laine, Vol. 14 (Oxford University Press, New York, 1988), p. 14.
[40] R. Abrines and I. C. Percival, Proc. Phys. Soc. **88**, 861 (1966).
[41] R. E. Olson and A. Salop, Phys. Rev. A **16**, 531 (1977).
[42] C. O. Reinhold and C. A. Falcon, Phys. Rev. A **33**, 3859 (1986).
[43] V. J. Montemayor and G. Schiwietz, Phys. Rev. A **40**, 6223 (1989).
[44] L. Meng, C. O. Reinhold, and R. E. Olson, Phys. Rev. A **40**, 3637 (1989).
[45] S. Otranto and R. E. Olson, Phys. Rev. A **77**, 022709 (2008).
[46] C. J. Wood and R. E. Olson, Phys. Rev. A **59**, 1317 (1999).
[47] G. Herzberg, *Molecular Spectra and Molecular Structure*, Vol. 1 (Van Nostrand, New York, 1950).
[48] A. E. S. Green, D. L. Sellin, and A. S. Zachor, Phys. Rev. **184**, 1 (1969).
[49] R. H. Garvey, C. H. Jackman, and A. E. S. Green, Phys. Rev. A **12**, 1144 (1975).
[50] D. R. Schultz, P. C. Stancil, and M. J. Rakovic, J. Phys. B **34**, 2739 (2001).
[51] A. D. MacKellar and R. L. Becker, J. Phys. B **17**, 3923 (1984).
[52] F. J. de Heer, J. Schutten, and H. Moustafa, Physica (Amsterdam) **32**, 1973 (1966).
[53] *Atomic Data for Controlled Fusion Research*, ORNL Report No. 5206, Vol. 1, C. F. Barnett, J. A. Ray, E. Ricci, and M. I. Wilker, Oak Ridge National Laboratory, E. W. McDaniel and E. W. Thomas (Georgia Institute of Technology and H. B. Gilbody, Queen's University, Belfast, 1977).
[54] H. A. Bethe and E. E. Salpeter, *Quantum Mechanics of One- and Two-Electron Atoms* (Plenum, New York, 1977).
[55] B. H. Bransden and C. J. Joachain, *Physics of Atoms and Molecules* (Longman Scientific & Technical/Wiley, New York, 1983).
[56] T. E. Sharp, At. Data **2**, 119 (1971).
[57] V. D. Rodriguez, Y. D. Wang, and C. D. Lin, Phys. Rev. A **52**, R9 (1995).
[58] R. E. Olson, Phys. Rev. A **24**, 1726 (1981).
[59] S. Otranto and R. E. Olson, J. Phys. B **43**, 144004 (2010).
[60] R. Bracewell, in *The Fourier Transform and Its Applications*, 3rd ed. (McGraw-Hill, New York, 2000), p. 351.
[61] V. Mergel *et al.*, Phys. Rev. Lett. **74**, 2200 (1995).
[62] W. C. Keever and E. Everhart, Phys. Rev. **150**, 43 (1966).
[63] W. L. Hodge, A. L. Goldberger, M. Vedder, and E. Pollack, Phys. Rev. A **16**, 2360 (1977).
[64] R. S. Gao, L. K. Johnson, C. L. Hakes, K. A. Smith, and R. F. Stebbings, Phys. Rev. A **41**, 5929 (1990).
[65] L. D. Landau, Phys. Sov. Union **2**, 46 (1932).
[66] C. Zener, Proc. R. Soc. London, Ser. A **137**, 696 (1932).
[67] Y. N. Demkov, Zh. Eksp. Teor. Fiz. **45** (1963) [Sov. Phys. JETP **18**, 138 (1964)].
[68] R. Cabrera-Trujillo, Y. Öhrn, E. Deumens, J. R. Sabin, and B. G. Lindsay, Phys. Rev. A **66**, 042712 (2002).
[69] R. S. Gao, L. K. Johnson, G. J. Smith, C. L. Hakes, K. A. Smith, N. F. Lane, R. F. Stebbings, and M. Kimura, Phys. Rev. A **44**, 5599 (1991).